HHS Public Access

Author manuscript

Ind Eng Chem Res. Author manuscript; available in PMC 2019 April 05.

Published in final edited form as:

Ind Eng Chem Res. 2018 June 13; 57(23): 7826–7833. doi:10.1021/acs.iecr.7b04732.

Advancement in Photothermal Effect of Carbon Nanotubes by Grafting of Poly(amidoamine) and Deposition of CdS Nanocrystallites

Gururaj M. Neelgund and **Aderemi Oki***

Department of Chemistry, Prairie View A&M University, Prairie View, Texas 77446, United States

Abstract

A robust, near-infrared (NIR) active photothermal agent, CNTs-PAMAM/G4-CdS, is designed by covalent grafting of fourth generation poly(amidoamine) (PAMAM) to carbon nanotubes (CNTs) and successive deposition of cadmium sulfide (CdS) nanocrystallites. The systematic advancement in photothermal effect of CNTs was achieved by grafting of first, second, third, and fourth generation PAMAM through the repeated process of Michael's addition. The subsequent deposition of CdS nanocrystallites over fourth generation PAMAM grafted CNTs has further improved the photothermal effect (PTE) of CNTs. The photothermal effect of CNTs-PAMAM/G4-CdS was accessed by illuminating with 980 nm NIR laser. During measurement of PTE, maximum temperature attained by CNTs-PAMAM/G4-CdS was 64.1 °C which far exceeds the survival temperature of cancer cells. The photothermal conversion efficiency estimated for CNTs-PAMAM/G4-CdS was 32%, which is higher than the value reported for popular gold and copper based photothermal agents. Apart from its outstanding photothermal effect, CNTs-PAMAM/G4-CdS possessed excellence in both antiphoto-bleaching and antiphoto-corrosiveness.

Graphical Abstract

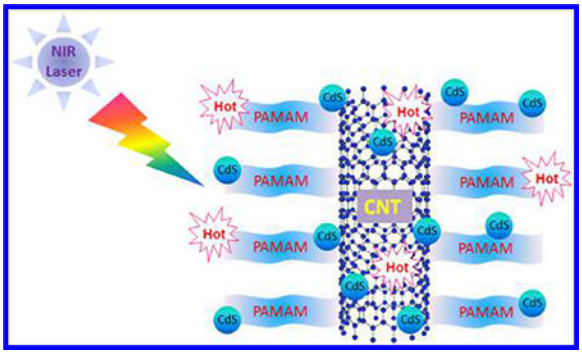

*Corresponding Author aroki@pvamu.edu (A.O.).

The authors declare no competing financial interest.

ASSOCIATED CONTENT

Supporting Information

The Supporting Information is available free of charge on the ACS Publications website at DOI: 10.1021/acs.iecr.7b04732.

Photothermal effect of CNTs-PAMAM/G4-CdS at different concentrations; XRD patterns of CNTs-PAMAM/G4-CdS (PDF)

1. INTRODUCTION

Generally, early stage detected cancer is treated by surgery, and if it is detected during its middle or later stages, it is treated with radio or chemotherapeutic techniques.[1] However, both of these radio or chemotherapeutic methods have major drawbacks of severe intrinsic side effects on normal tissue, inferior selectivity, and drug resistance.[1] So, due to adverse effects associated with these therapies, photomediated therapy, viz., photothermal therapy (PTT), has recently attained a great deal of attention owing to its exceptional benefits.[2] PTT offers distinctive advantages like precise delivery of energy to targeted cancer cells selectively without damage to healthy tissues.[3] The principle of PTT is employment of heat generated by an adopted platform under exposure to near-infrared (NIR) radiation in the destruction of cancer cells. In the electromagnetic spectrum, the NIR region is known as a biological window as the absorption ability by body tissue of NIR radiation is relatively low. In addition, NIR radiation is able to penetrate about 10–30 mm inside the skin, which is higher than the penetration rate of far-infrared radiation.[4] On account of this, PTT has attained a key importance and its success merely depends on the photothermal agent applied in therapy. It means the employed photothermal agent should possess high absorption ability to NIR radiation and elevated efficiency in converting it to heat or thermal energy. Compared to the popularly known photothermal agents, carbon nanotubes (CNTs) composites are particularly interesting because of their unique structural and physical properties. The CNTs are known for their high absorption capability to NIR radiation and efficient conversion to localized heat that can cause the death of cancer cells.[5–8] Therefore, CNTs mediated PTT has been applied in treating a variety of cancers.[9] The photothermal conversion efficiency of CNTs is more than that of the popularly known photothermal agents such as gold nanoparticles.[10] Moreover, the absorbance coefficient of CNTs to NIR radiation is about 300%, and their photon-to-heat conversion efficiency is three times higher than gold.[4,11] Usually, the diameter of CNTs is lower than the diameter of most of the gold nanoparticles, so by using CNTs, it is possible to destroy cancer cells with high precision. However, their low biocompatibility, insolubility in water, and elevated toxicity hampered the full pledged application of CNTs in PTT. Nonetheless, these properties of CNTs could be manipulated by proper surface functionalization to customize for their safe use in PTT.[12–14] To functionalize CNTs, several polymers have been reported; among those, poly(amidoamine) (PAMAM) is especially attractive in consideration of its uncompromised properties and outstanding biocompatibility.[15–18] To date, PAMAM has been extensively explored as a carrier for drug and gene delivery owing to its exceptional nanoscale architecture and multifunctionality.[19,20] However, PAMAM has been the least applied in PTT even with its excellent biocompatibility. Thus, exploration of potential employment of PAMAM in PTT is a current major need.

Cadmium sulfide (CdS) is an important II–VI group chalcogenide semiconductor with direct and narrow band gap of 2.4 eV, and it persists with superior photoconductivity, electronic band gap tuning capability, and high electron affinity.[21–23] Moreover, CdS has large exciton binding energy of ~28 meV; therefore, high efficient excitonic processes are expected in CdS, and these processes could directly influence and improve the optical properties of CdS.[24] On account of its high photoabsorption coefficient, CdS holds great potential in

optoelectronics, photocatalysis, solar energy conversion, and X-ray detectors.[25–27] Besides, CdS has found application in the biomedical field ranging from antibacterial to molecular histopathology, advanced disease diagnostics, and biological imaging.[28,29] Nevertheless, its low absorption to NIR radiation compared to UV and visible radiation has restricted the use of CdS in therapies. Hence, a suitable functionalization is critical to make CdS NIR active, and it can be attained through conjugation of CdS with outstanding materials, viz., CNTs and PAMAM. Accordingly, we developed a robust photothermal agent, CNTs-PAMAM/G4-CdS, through deposition of CdS nanocrystallites over fourth generation (G4) PAMAM grafted CNTs. Thus, prepared CNTs-PAMAM/G4-CdS is verified as a photothermal agent by measuring its phothermal effect under exposure to a 980 nm NIR laser.

2. EXPERIMENTAL SECTION

2.1. Materials.

All the reagents were purchased from Sigma-Aldrich and used without further purification unless otherwise noted, and the aqueous solutions were prepared using ultrapure water obtained from a Milli-Q Plus system (Millipore).

2.2. Preparation of CNTs-PAMAM/G4-CdS.

Prior to grafting of PAMAM, pristine CNTs were modified to carboxylated and acylated CNTs.[27] Then, acylated CNTs were employed in covalent grafting of fourth generation (G4) PAMAM using the repeated process of Michael addition by methyl methacrylate to the surface amino groups and amidation of terminal ester groups with ethylenediamine.[27] Successively, CdS nanocrystals were deposited over PAMAM/G4 grafted CNTs (CNTs-PAMAM/G4) by dispersing in 25 mL of methanol and addition of cadmium acetate (0.01 mol L^{-1}). Then, 20 mL of Na_2S in methanol (0.01 mol L^{-1}) was added, and the resulting mixture was stirred under ambient condition for 6 h to yield CNTs-PAMAM/G4-CdS.

2.3. Photothermal Effect.

The photothermal effect (PTE) of the samples was evaluated using a 980 nm NIR diode laser system (Armlaser Inc. USA) with an output power of 2 W/cm^2. In each experiment, 1 mL of aqueous dispersion of the sample was transferred into a 1 × 1 × 4 cm^3 quartz cuvette and illuminated with the NIR laser. The resulting elevation in temperature mediated by the exposure to NIR radiation was measured using a Hanna precision digital thermometer (Model: HI93510) with a thermocouple immersed in the aqueous dispersion of sample during the experiment.

2.4. Characterization.

The UV–vis–NIR absorption spectra of the samples were obtained using a Jasco V-770 spectrophotometer, and Fourier transform infrared (FT-IR) spectra were recorded using a Thermo-Nicolet IR 2000 spectrometer with KBr pellet. XRD patterns were acquired by a Scintag X-ray diffractometer (PAD X), equipped with Cu Kα photon source (45 kV, 40 mA) at a scanning rate of 3° min^{-1}. X-ray photoelectron spectra (XPS) were recorded by a PerkinElmer PHI 5600 ci X-ray photoelectron spectrometer.

3. RESULTS AND DISCUSSION

The FT-IR spectrum of CNTs-PAMAM/G4 (Figure 1a) displayed the important characteristic bands persist for PAMAM and CNTs. Among these, a broad band due to N-H stretching vibrations appeared at 3440 cm^{-1}, and the bands of amide (-CO-NH-) I and II were found at 1649 and 1516 cm^{-1}, respectively. In addition, the characteristic bands of CNTs, viz., aromatic C-C, C=C, -CH, and C-H paraaromatic out of plane vibration, appeared at 1520, 1380, 1110, and 837 cm^{-1}, respectively.[27,28,30] The spectrum of CNTs-PAMAM/G4-CdS (Figure 1b) demonstrated the significant characteristic bands displayed in CNTs-PAMAM/G4; obvious modifications are associated with shifting of the bands' position and their diminished intensity. This proposes that the structure of CNTs-PAMAM/G4 was not directly affected and ruined in CNTs-PAMAM/G4-CdS by deposition of CdS nanocrystallites. In addition, it indicates the strong interaction persists between CNTs-PAMAM/G4 and CdS nanocrystallites. The XRD pattern of CNTs-PAMAM/G4 (Figure 2a) exhibited the typical characteristic diffraction peaks at 26.1° and 42.6° generated by (0 0 2) and (1 0 0) planes of hexagonal graphitic shells of CNTs,[31] while CNTs-PAMAM/G4-CdS (Figure 2b) displayed two broad bands at 26.5° and 47.0°, in which the former band at 26.5° was due to the fusing of the (1 1 1) plane of cubic CdS and the (0 0 2) plane of CNTs. The following band at 47.0° was expected to be two distinct bands at 43.8° and 51.7° owing to (2 2 0) and (3 1 1) planes of CdS, respectively (JCPDS 75–0581); instead, these bands were merged and became a single wide band due to the nanometer size of CdS crystallites. The possibility of this kind of behavior is depicted in literature.[27,28,32] Furthermore, the crystallite size of CdS in CNTs-PAMAM/G4-CdS was calculated using Debye–Scherrer equation and found to be 1.4 nm.[33]

The UV–vis–NIR spectrum of CNTs-PAMAM/G4 (Figure 3a) showed an absorption band at 237 nm, consistent with C=C bonds of CNTs.[27] In addition, absorption due to PAMAM in CNTs-PAMAM/G4 was observed at 257 nm.[34] In the spectrum of CNTs-PAMAM/G4-CdS (Figure 3b), absorption bands of CNTs and PAMAM have combined and are revealed as a single band at 241 nm. Apart, a shoulder band appeared for CNTs-PAMAM/G4-CdS at 460 nm due to presence of CdS nanocrystallites.[35] Overall, both CNTs-PAMAM/G4 and CNTs-PAMAM/G4-CdS have possessed significant absorption in the NIR region around 970 nm, and it indicates the potential application of CNTs-PAMAM/G4 and CNTs-PAMAM/G4-CdS as strong NIR active PTE agents. However, to verify the chemical composition and electronic state of CNTs-PAMAM/G4-CdS, its XPS was measured and spectra are illustrated in Figure 4. The survey spectra of CNTs-PAMAM/G4-CdS (Figure 4a) show the presence of C, O, N, Cd, and S elements. In order to determine the chemical state of these elements, high resolution spectra were recorded. The peak with binding energy of 284.5 eV in the spectrum of C 1s (Figure 4b) is ascribed to graphitic carbon (C=C bonds) and C-C bonds of CNTs.[36] The peak found at 532.0 eV in the spectrum of O 1s (Figure 4c) was attributed to -COO bonds.[37] The spectrum of Cd 3d (Figure 4d) displayed the doublet featured Gaussian peaks due to spin–orbit splitting at 405.8 and 412.5 eV corresponding to Cd 3d5/2 and Cd 3d3/2, respectively, with a spin–orbit separation of 6.7 eV.[37] These peaks reveal the existence of divalent Cd (Cd^{2+}) ions in CdS nanocrystallites. Generally, Cd 3d levels of nanocrystallites provide a single peak feature in each of the spin–orbit components

without any evidence for a second Cd species, which is in close proximity with the XPS spectrum of nanosized bulk CdS.[38,39] This suggests entire Cd sites are basically equivalent in an identical chemical environment, and they bonded to S without any extraneous impurities. The spectrum of S 2p (Figure 4e) demonstrated a peak at 161.9 eV, which is indexed to S 2p3/2 of sulfide exists in CdS nanocrystallites.[37] Moreover, the peak observed in the spectrum of N 1s (Figure 4f) shows the presence of nitrogen in CNTs-PAMAM/G4-CdS, which is originated by PAMAM.

Inspired by significant absorption of CNTs-PAMAM/G4-CdS in the NIR region, its PTE with aqueous dispersion was measured at its concentration level of 1 mg/mL and quantified by comparing it with the PTE of CNTs-PAMAM/G4, CNTs, and water. Figure 5 details the NIR induced temperature rise obtained by exposure to the 980 nm laser. The maximum temperature attained by water at its continuous illumination for 7 min was 28.5 °C, and it persists with a total rise in temperature (ΔT) of 8.1 °C (Table 1). A significant amplification (ΔT) of 29.2 °C was observed for CNTs with a maximum temperature of 50.0 °C. The PTE of water is very low, so that, PTE measured for aqueous dispersion of CNTs was mainly contributed by the CNTs without any major contribution from water. The PTE of CNTs was further systematically improved in a stepwise manner by covalent grafting of first, second, third, and fourth generation PAMAM. It was shown that PTE of CNTs was elevated from 29.5 to 32.9 °C (ΔT) by grafting of first generation PAMAM (CNTs-PAMAM/G1). It was further improved to 34.8 °C for second generation (CNTs-PAMAM/G2) and subsequently raised to 38.2 °C in third generation (CNTs-PAMAM/G3). Successively, PTE has risen to 41.8 °C for fourth generation PAMAM (CNTs-PAMAM/G4) with a maximum temperature of 62.1 °C. Further, the deposition of CdS nanocrystallites rapidly enhanced the PTE of CNTs-PAMAM/G4 in CNTs-PAMAM/G4-CdS. The temperature of CNTs-PAMAM/G4-CdS was increased from 20.7 to 64.1 °C, by 7 min of irradiation, and there was a difference in temperature (ΔT) of 43.4 °C. Thus, the NIR photoinduced heat generation ability of CNTs was methodically improved by grafting of PAMAM and subsequent deposition of CdS nanocrystallites. The excellence in PTE of CNTs-PAMAM/G4-CdS was further verified by calculating its photothermal conversion efficiency (η) using Roper's method, eq 1,[40–45]

$$\eta = \frac{hS\left(T_{\max} - T_{\text{surr}}\right) - Q_{\text{dis}}}{I\left(1 - 10^{-A_{980}}\right)} \quad (1)$$

where η is the photothermal efficiency, h is heat transfer coefficient, and S is the surface area of the sample container. $T_{\max}$ is the maximum temperature attained by the sample, and T_{surr} is the surrounding temperature (Table 2). I is the power of the laser source (2000 mW), and A_{980} is the absorbance of aqueous dispersion of samples at an excitation wavelength of 980 nm. Q_{dis} is the rate of heat dissipated due to absorption of light by the solvent and the container.

To calculate the value of hS, a dimensionless driving force of temperature, θ is introduced and scaled using the maximum system temperature, $T_{\max}$, and the surrounding temperature, T_{surr}.

$$\theta = \frac{T - T_{surr}}{T_{max} - T_{surr}} \quad (2)$$

The sample system time constant, τs, was evaluated using eq 3

$$t = -\tau s \ln(\theta) \quad (3)$$

The value of τs was calculated using Figures 6 and 7 and found to be 421 and 302 s for CNTs-PAMAM/G4 and CNTs-PAMAM/G4-CdS, respectively. Using the value of τs, unknown parameter hS was evaluated with eq 4.

$$hS = \frac{m_D C_D}{\tau s} \quad (4)$$

where m_D is the mass of DI water (1.01 g) and C_D is its heat capacity. The value of Q_{dis} was measured separately using a quartz cuvette containing only DI water without any sample, and it was found to be 25.9 mW.

Then, the photothermal conversion efficiency (η) calculated for CNTs-PAMAM/G4 and CNTs-PAMAM/G4-CdS was found to be 23% and 32%, respectively. The photothermal conversion efficiency estimated for both CNTs-PAMAM/G4 and CNTs-PAMAM/G4-CdS is higher than the value reported for popular photothermal agents, viz., Au nanoshells (18%),[46] Au nanorods (22%),[47] $Cu_{2-x}Se$ nanoparticles (22%),[48] Au nanoshells (25%),[43] and Cu_9S_5 nanoparticles (25.7%).[49] Therefore, CNTs-PAMAM/G4 and CNTs-PAMAM/G4-CdS could be promising PTE agents in the future as both of these possessed higher photothermal conversion efficiency than traditional PTE agents. However, the maximum temperature attained during the measurement of PTE by CNTs-PAMAM/G4 and CNTs-PAMAM/G4-CdS was 62.1 and 64.1 °C, respectively. This temperature far exceeds the temperature tolerance level of cancer cells of 50 °C.[49,50] Therefore, the elevation in temperature exhibited by CNTs-PAMAM/G4 and CNTs-PAMAM/G4-CdS is adequate to induce the death of tumoral or cancer cells.

Apart from 1 mg/mL, the PTE of CNTs-PAMAM/G4-CdS was determined at its concentrations of 0.5 and 0.25 mg/mL. The PTE of CNTs-PAMAM/G4-CdS was proportional to its concentration and attained a linear improvement with respect to an increase in concentration (Figure S1). The ΔT of 40.4, 42.0, and 43.4 °C was recorded for 0.25, 0.5, and 1 mg/mL of CNTs-PAMAM/G4-CdS, respectively. Instead of its excellent PTE, CNTs-PAMAM/G4-CdS exhibited outstanding antiphoto-bleaching and antiphoto-corrosive properties, which was verified by measuring the PTE for a successive five cycles. It was found that, for all the measured five cycles, PTE of CNTs-PAMAM/G4-CdS was virtually constant (Figure 8). Moreover, CNTs-PAMAM/G4-CdS showed an exceptional structural stability, and it was accessed by recording the XRD pattern of CNTs-

PAMAM/G4-CdS before and after its application in five cycles (Figure S2). It was revealed that the structure of CNTs-PAMAM/G4-CdS was not ruined after its employment for five times.

4. CONCLUSIONS

In conclusion, a systematic increment in PTE of CNTs was attained by covalent grafting of first, second, third, and fourth generation PAMAM and successive deposition of CdS nanocrystallites. Both CNTs-PAMAM/G4 and CNTs-PAMAM/G4-CdS have possessed outstanding photothermal conversion efficiencies of 23% and 32%, respectively, which are higher than the value reported for popular photothermal agents, viz., gold and copper nanomaterials. The temperature attained by CNTs-PAMAM/G4-CdS by irradiating with a 980 nm laser for 7 min was 64.1 °C, which far exceeds the temperature survival rate of cancer cells. Thus, CNTs-PAMAM/G4-CdS could be an efficient photothermal agent to employ in future PTT. Not limited to its exceptional PTE, CNTs-PAMAM/G4-CdS possessed excellent antiphoto-bleaching and antiphoto-corrosive properties as well, and its structure was not ruined after its application in five consecutive cycles. The PTE of CNTs-PAMAM/G4-CdS was found to be proportional to its concentration. In consideration of its significant performance and vital properties, CNTs-PAMAM/G4-CdS could be an ideal replacement for current photothermal agents to enhance the performance of PTT in the future.

Supplementary Material

Refer to Web version on PubMed Central for supplementary material.

ACKNOWLEDGMENTS

Authors acknowledge the support from NIH-NIGMS grant 1SC3GM121229-01 and the department grant L0002 from Welch Foundation, Texas, United States.

REFERENCES

(1). Wang D; Ren Y; Shao Y; Yu D; Meng L Facile Preparation of Doxorubicin-Loaded and Folic Acid-Conjugated Carbon Nanotubes@Poly(N-vinyl pyrrole) for Targeted Synergistic Chemo-Photothermal Cancer Treatment. Bioconjugate Chem. 2017, 28, 2815–2822.

(2). Phillips D Light Relief. Photochem. Photobiol. Sci 2010, 9, 1589–1596. [PubMed: 21082123]

(3). Luo S; Yang Z; Tan X; Wang Y; Zeng Y; Wang Y; Li C; Li R; Shi C Multifunctional Photosensitizer Grafted on Polyethylene Glycol and Polyethylenimine Dual-Functionalized Nanographene Oxide for Cancer-Targeted Near-Infrared Imaging and Synergistic Phototherapy. ACS Appl. Mater. Interfaces 2016, 8, 17176–17186. [PubMed: 27320692]

(4). Han S; Kwon T; Um J; Haam S; Kim W Highly Selective Photothermal Therapy by a Phenoxylated-Dextran-Functionalized Smart Carbon Nanotube Platform. Adv. Healthcare Mater 2016, 5, 1147–1156.

(5). Zhang M; Wang W; Wu F; Yuan P; Chi C; Zhou N Magnetic and Fluorescent Carbon Nanotubes for Dual Modal Imaging and Photothermal and Chemo-therapy of Cancer Cells in Living Mice. Carbon 2017, 123, 70–83.

(6). Eldridge BN; Bernish BW; Fahrenholtz CD; Singh R Photothermal Therapy of Glioblastoma Multiforme Using Multi-walled Carbon Nanotubes Optimized for Diffusion in Extracellular Space. ACS Biomater. Sci. Eng 2016, 2, 963–976. [PubMed: 27795996]

(7). Liang X; Shang W; Chi C; Zeng C; Wang K; Fang C; Chen Q; Liu H; Fan Y; Tian J Dye-conjugated Single-walled Carbon Nanotubes Induce PhotothermalTherapyUnder the Guidance of Near-infrared Imaging. Cancer Lett. 2016, 383, 243–249. [PubMed: 27693557]

(8). Dong X; Sun Z; Wang X; Leng X An Innovative MWCNTs/DOX/TC Nanosystem for Chemo-photothermalCombinationTherapy of Cancer. Nanomedicine 2017, 13, 2271–2280. [PubMed: 28712919]

(9). Zhang P; Hu C; Ran W; Meng J; Yin Q; Li Y Recent Progress in Light Triggered Nanotheranostics for Cancer Treatment. Theranostics 2016, 6, 948–68. [PubMed: 27217830]

(10). Chatterjee DK; Diagaradjane P; Krishnan S Nanoparticle-Mediated Hyperthermia in Cancer Therapy. Ther. Delivery 2011, 2, 1001–1014.

(11). Robinson JT; Welsher K; Tabakman SM; Sherlock SP; Wang H; Luong R; Dai H High Performance in vivo Near-IR (>1 μm) Imaging and Photothermal Cancer Therapy with Carbon Nanotubes. Nano Res. 2010, 3, 779–793. [PubMed: 21804931]

(12). Kostarelos K; Bianco A; Prato M Promises, Facts and Challenges for Carbon Nanotubes in Imaging and Therapeutics. Nat. Nanotechnol 2009, 4, 627–633. [PubMed: 19809452]

(13). Bardi G; Nunes A; Gherardini L; Bates K; Al-Jamal KT; Gaillard C; Prato M; Bianco A; Pizzorusso T; Kostarelos K Functionalized Carbon Nanotubes in the Brain: Cellular Internalization and Neuro inflammatory Responses. PLoS One 2013, 8, e80964. [PubMed: 24260521]

(14). Bussy C; Al-Jamal KT; Boczkowski J; Lanone S; Prato M; Bianco A; Kostarelos K Microglia Determine Brain Region-Specific Neurotoxic Responses to Chemically Functionalized Carbon Nanotubes. ACS Nano 2015, 9, 7815–7830. [PubMed: 26043308]

(15). Peng Q; He X; Li Y; Wang C; Wang R; Hu P; Yan Y; Sritharan T Chemically and Uniformly Grafting Carbon Nanotubes onto Carbon Fibers by Poly(amidoamine) for Enhancing Interfacial Strength in Carbon Fiber Composites. J. Mater. Chem 2012, 22, 5928–5931.

(16). Peng Q; Li Y; He X; Lv H; Hu P; Shang Y; Wang C; Wang R; Sritharan T; Du S Interfacial Enhancement of Carbon Fiber Composites by Poly(amidoamine) Functionalization. Compos. Sci. Technol 2013, 74, 37–42.

(17). Li Y; Peng Q; He X; Hu PA; Wang C; Shang Y; Wang R; Jiao W; Lv H Synthesis and Characterization of a New Hierarchical Reinforcement by Chemically Grafting Graphene Oxide onto Carbon Fiber. J. Mater. Chem 2012, 22, 18748–18752.

(18). Bertero A; Boni A; Gemmi M; Gagliardi M; Bifone A; Bardi G Surface Functionalisation Regulates Polyamidoamine Dendrimer Toxicity on Blood–brain Barrier Cells and the Modulation of Key Inflammatory Receptors on Microglia. Nanotoxicology 2014, 8, 158–168. [PubMed: 23298388]

(19). Saraswathy M; Knight GT; Pilla S; Ashton RS; Gong S Multifunctional Drug Nanocarriers Formed by cRGD-conjugated βCD-PAMAM-PEG for Targeted Cancer Therapy. Colloids Surf., B 2015, 126, 590–597.

(20). Kesharwani P; Jain K; Jain NK Dendrimer as Nanocarrier for drug delivery. Prog. Polym. Sci 2014, 39, 268–307.

(21). Li Q; Li X; Wageh S; Al-Ghamdi AA; Yu J CdS/Graphene Nanocomposite Photocatalysts. Adv. Energy Mater 2015, 5, 1500010–1500038.

(22). Peng Q; Xue D; Zhan S; Ni C Visible-light-driven Photocatalytic System Based on a Nickel Complex over CdS Materials for Hydrogen Production from Water. Appl. Catal., B 2017, 219, 353–361.

(23). Pandya S; Raval K Investigation of Structural, Morphological and Optical Properties of Cadmium Sulphide (CdS) Thin Films at Different Cd/S Concentration Deposited by Chemical Technique. J. Mater. Sci.: Mater. Electron 2017, 28, 18031–18039.

(24). Liu X; Zhang Q; Xing G; Xiong Q; Sum TC Size-Dependent Exciton Recombination Dynamics in Single CdS Nanowires beyond the Quantum Confinement Regime. J. Phys. Chem. C 2013, 117, 10716–10722.

(25). Muniyappan S; Solaiyammal T; Keerthana BGT; Vivek P; Murugakoothan P Influence of Annealing Temperature on Structural, Morphological and Optical Properties of CTAB Assisted

Cadmium Sulphide (CdS) Quantum Dots: Promising Candidate for Quantum Dot Sensitized Solar Cell (QDSSC) Applications. J. Mater. Sci.: Mater. Electron 2017, 28, 11317–11324.

(26). Sun ZP; Zhang XG; Liang YY; Li HL Highly Dispersed Pd Nanoparticles on Covalent Functional MWNT Surfaces for Methanol Oxidation in Alkaline Solution. Electrochem. Commun 2009, 11, 557–561.

(27). Neelgund GM; Oki A Photocatalytic activity of CdS and Ag2S Quantum Dots Deposited on Poly(amidoamine) Functionalized Carbon Nanotubes. Appl. Catal., B 2011, 110, 99–107. [PubMed: 22267895]

(28). Neelgund GM; Oki A; Luo Z Antimicrobial Activity of CdS and Ag2S Quantum Dots Immobilized on Poly(amidoamine) Grafted Carbon Nanotubes. Colloids Surf., B 2012, 100, 215–221.

(29). Durga B; Raziya S; Rajmahanti SG; Govindh B; Raju KV; Annapurna N Synthesis and Characterization of Cadmium Sulphide Nanoparticles Using Annona Muricata Leaf Extract as Reducing/Capping Agent. Chem. Sci. Trans 2016, 5, 1035–1041.

(30). Sun ZP; Zhang XG; Liang YY; Li HL Highly Dispersed Pd Nanoparticles on Covalent Functional MWNT Surfaces for Methanol Oxidation in Alkaline Solution. Electrochem. Commun 2009, 11, 557–561.

(31). Neelgund GM; Oki A Pd Nanoparticles Deposited on Poly(lactic acid) Grafted Carbon Nanotubes: Synthesis, Characterization and Application in Heck C–C Coupling Reaction. Appl. Catal., A 2011, 399, 154–160.

(32). Petkov V Nanostructure by High-energy X-ray Diffraction. Mater. Today 2008, 11, 28–28.

(33). Cullity BD Elements of X-Ray Diffraction; Edison-Wesley Publishing Company Inc.: Reading, MA, 1978.

(34). Balogh L; Tomalia DA Poly(Amidoamine) Dendrimer-Templated Nanocomposites. 1. Synthesis of Zerovalent Copper Nanoclusters. J. Am. Chem. Soc 1998, 120, 7355–7356.

(35). Weller H Colloidal Semiconductor Q-Particles: Chemistry in the Transition Region Between Solid State and Molecules. Angew. Chem., Int. Ed. Engl 1993, 32, 41–53.

(36). Cong Y; Li X; Qin Y; Dong Z; Yuan G; Cui Z; Lai X Carbon-doped TiO2 Coating on Multi-walled Carbon Nanotubes with Higher Visible Light Photocatalytic Activity. Appl. Catal., B 2011, 107, 128–134.

(37). Lv J; Li D; Dai K; Liang C; Jiang D; Lu L; Zhu G Multi-walled Carbon Nanotube Supported CdS-DETA nanocomposite for efficient Visible Light Photocatalysis. Mater. Chem. Phys 2017, 186, 372–381.

(38). Nanda J; Kuruvilla BA; Sarma DD Photoelectron Spectroscopic Study of CdS Nanocrystallites. Phys. Rev. B: Condens. Matter Mater. Phys 1999, 59, 7473–7479.

(39). Tseng C; Wang C; Chen C Modification of Multi-walled Carbon Nanotubes by Plasma Treatment and Further Use as Templates for Growth of CdS Nanocrystals. Nanotechnology 2006, 17, 5602–5612. [PubMed: 21727331]

(40). Roper DK; Ahn W; Hoepfner M Microscale Heat Transfer Transduced by Surface Plasmon Resonant Gold Nanoparticles. J. Phys. Chem. C 2007, 111, 3636–3641.

(41). Kam NWS; O'Connell M; Wisdom A; Dai H Carbon Nanotubes as Multifunctional Biological Transporters and Near-infrared Agents for Selective Cancer Cell Destruction. Proc. Natl. Acad. Sci. U. S. A. 2005, 102, 11600–11605. [PubMed: 16087878]

(42). Neelgund GM; Oki A Influence of Carbon Nanotubes and Graphene Nanosheets on Photothermal Effect of hydroxyapatite. J. Colloid Interface Sci 2016, 484, 135–145. [PubMed: 27599382]

(43). Tian Q; Jiang F; Zou R; Liu Q; Chen Z; Zhu M; Yang S; Wang J; Wang J; Hu J Hydrophilic Cu_9S_5Nanocrystals: a Photothermal Agent with a 25.7% Heat Conversion Efficiency for Photothermal Ablation of Cancer Cells in vivo. ACS Nano 2011, 5, 9761–9771. [PubMed: 22059851]

(44). Cui J; Jiang R; Xu S; Hu G; Wang L Cu7S4Nanosuperlattices with Greatly Enhanced Photothermal Efficiency. Small 2015, 11, 4183–4190. [PubMed: 25981697]

(45). Neelgund GM; Oki A Photothermal Effect: an Important Aspect for the Enhancement of Photocatalytic Activity Under Illumination by NIR Radiation. Mater. Chem. Front 2018, 2, 64–75.

(46). Huang P; Lin J; Li W; Rong P; Wang Z; Wang S; Wang X; Sun X; Aronova M; Niu G; Leapman RD; Nie Z; Chen X Biodegradable Gold Nanovesicles with an Ultrastrong Plasmonic Coupling Effect for Photoacoustic Imaging and Photothermal Therapy. Angew. Chem., Int. Ed 2013, 52, 13958–13964.

(47). Hessel CM; Pattani VP; Rasch M; Panthani MG; Koo B; Tunnell JW; Korgel BA Copper Selenide Nanocrystals for Photothermal Therapy. Nano Lett. 2011, 11, 2560–2566. [PubMed: 21553924]

(48). Pattani VP; Tunnell JW Nanoparticle-mediated Photothermal Therapy: a Comparative Study of Heating for Different Particle Types. Lasers Surg. Med 2012, 44, 675–684. [PubMed: 22933382]

(49). Ju E; Dong K; Liu Z; Pu F; Ren J; Qu X Tumor Microenvironment Activated Photothermal Strategy for Precisely Controlled Ablation of Solid Tumors Upon NIR Irradiation. Adv. Funct. Mater 2015, 25, 1574–1580.

(50). Yoo D; Jeong H; Noh SH; Lee JH; Cheon J Magnetically Triggered Dual Functional Nanoparticles for Resistance-Free Apoptotic Hyperthermia. Angew. Chem., Int. Ed 2013, 52, 13047–13051.

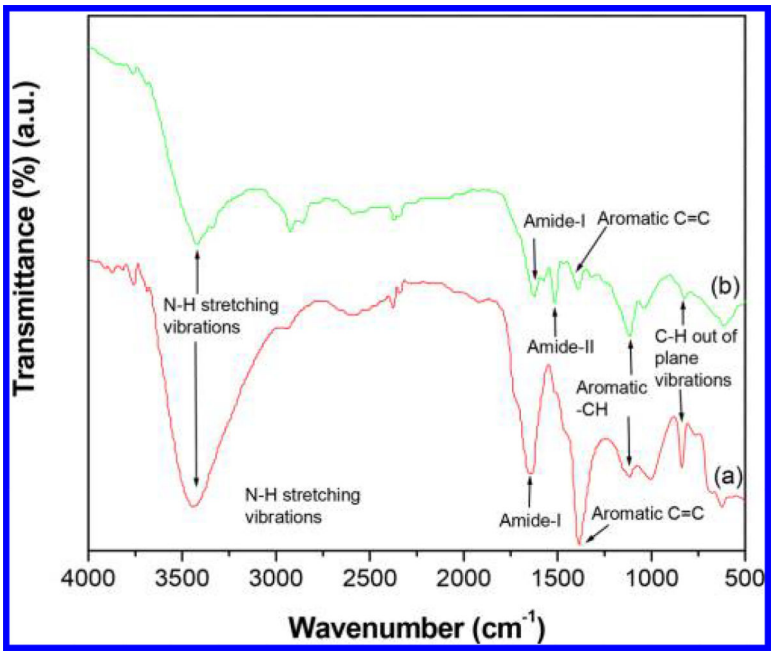

Figure 1.
FT-IR spectra of (a) CNTs-PAMAM/G4 and (b) CNTs-PAMAM/G4-CdS.

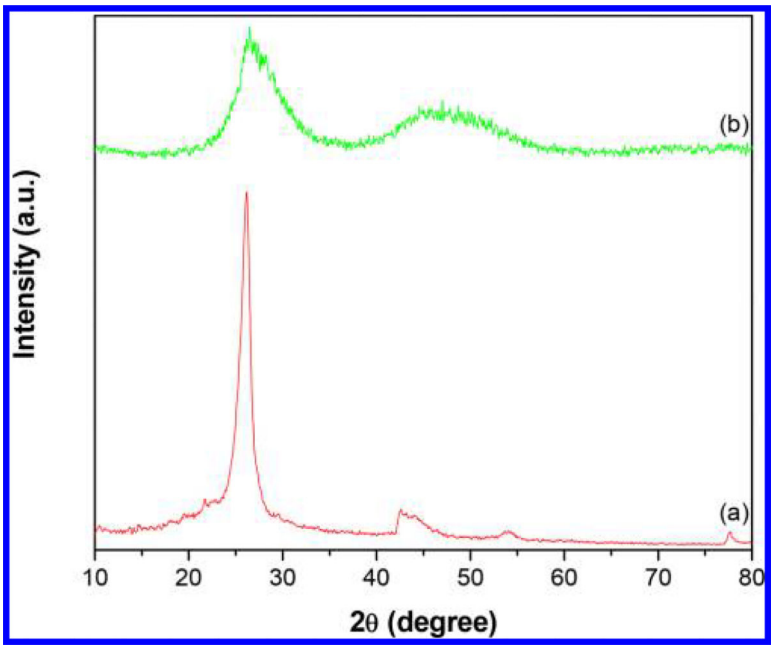

Figure 2.
XRD of (a) CNTs-PAMAM/G4 and (b) CNTs-PAMAM/G4-CdS.

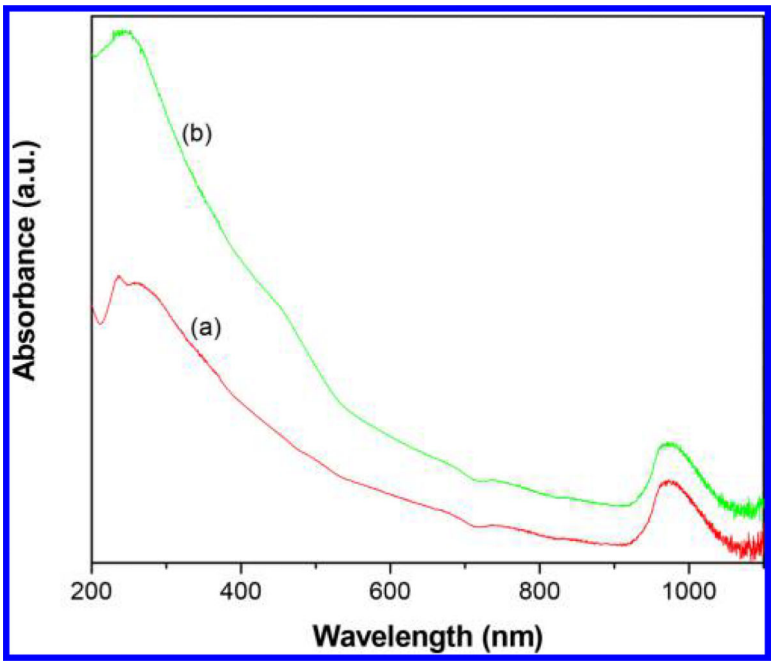

Figure 3.
UV–vis–NIR spectra of (a) CNTs-PAMAM/G4 and (b) CNTs-PAMAM/G4-CdS.

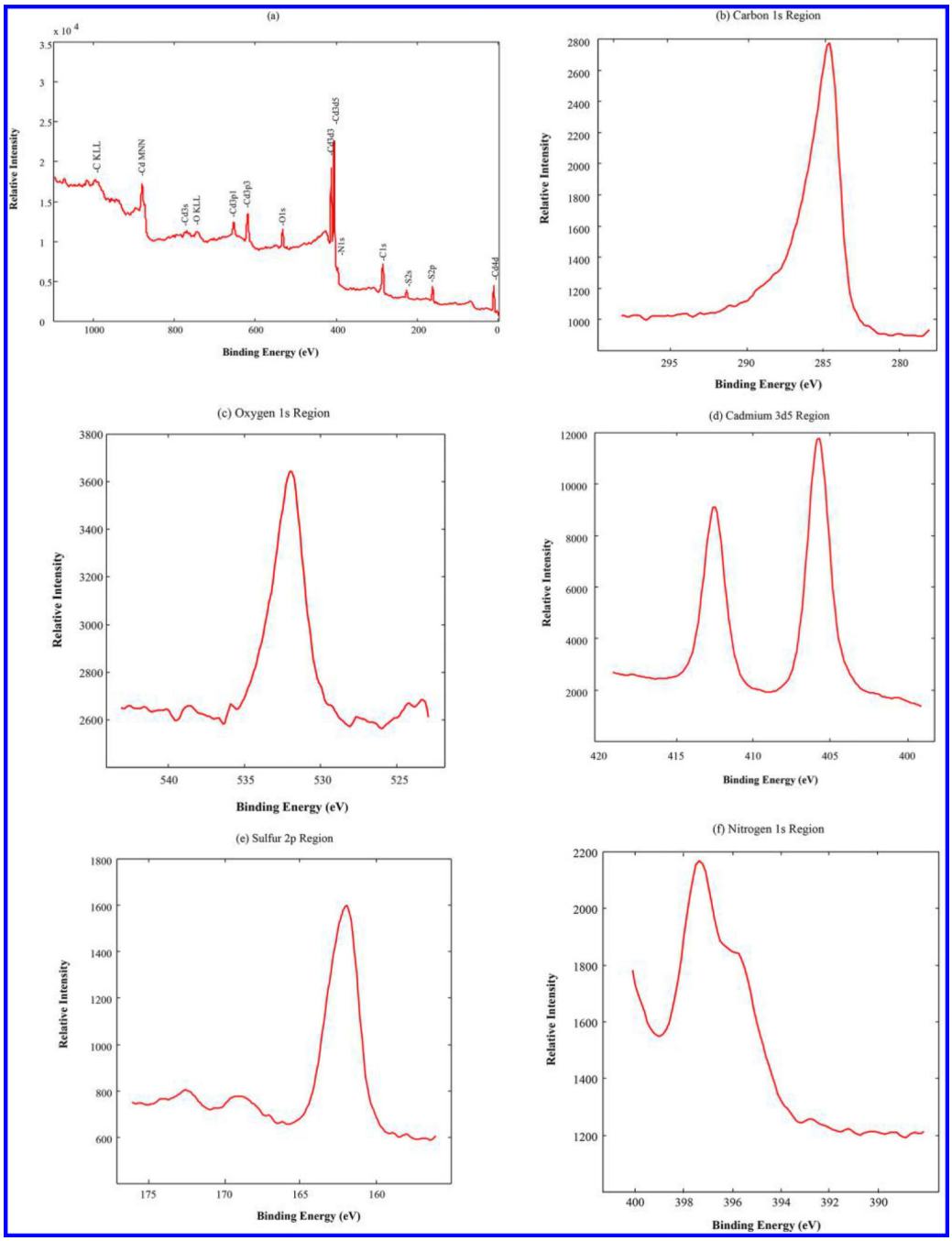

Figure 4.

(a) XPS survey spectrum of CNTs-PAMAM/G4-CdS and high resolution spectra of (b) C 1s, (c) O 1s, (d) Cd 3d5, (e) S 2p, and (f) N 1s.

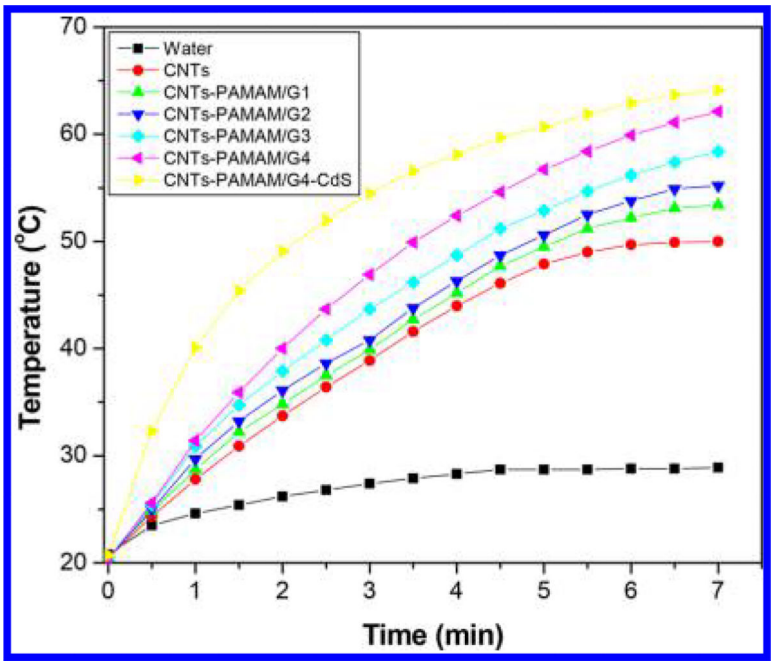

Figure 5.

Rise in temperature for aqueous dispersions of samples as a function of illumination under exposure to a 980 nm laser.

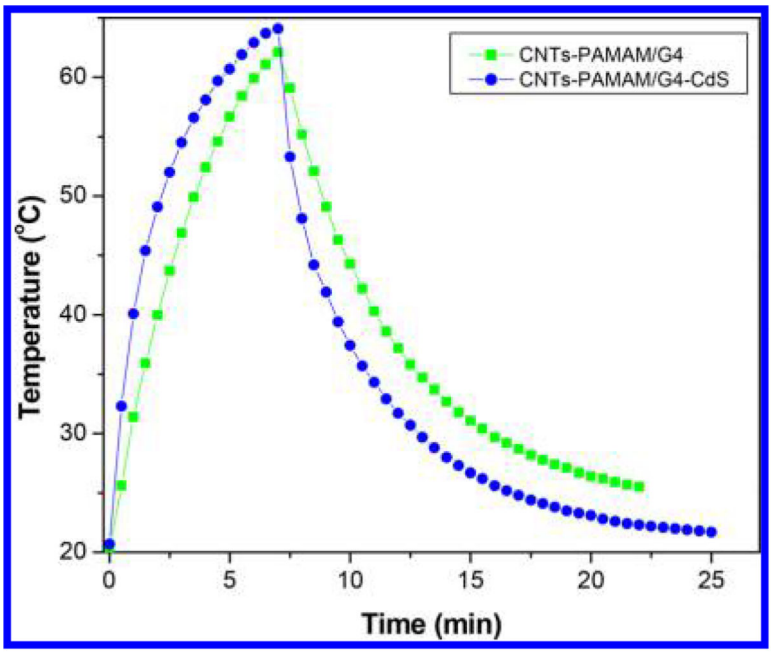

Figure 6.

Temperature variation found for aqueous dispersion of CNTs-PAMAM/G4 and CNTs-PAMAM/G4-CdS under exposure to a 980 nm laser followed by its shut off.

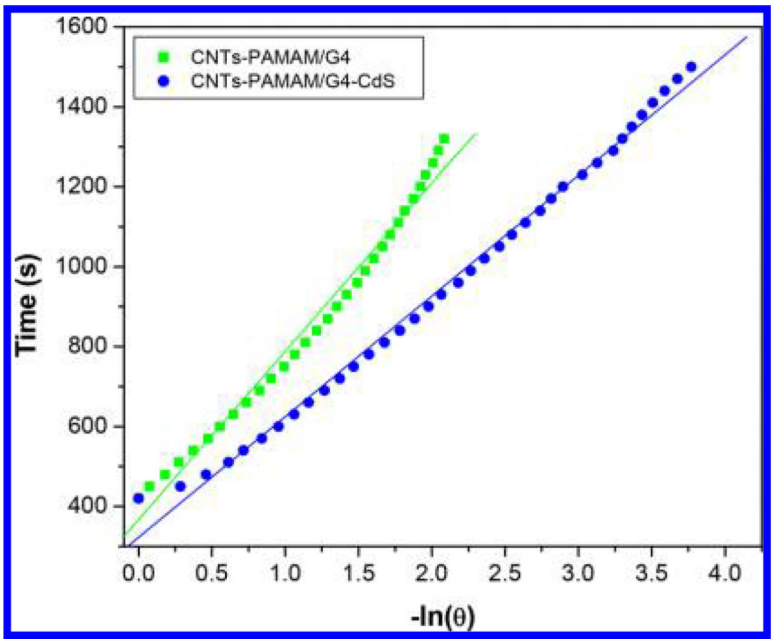

Figure 7.

Plot of time from cooling period versus negative natural logarithm of driving force temperature obtained for CNTs-PAMAM/G4 and CNTs-PAMAM/G4-CdS using the data shown in Figure 5.

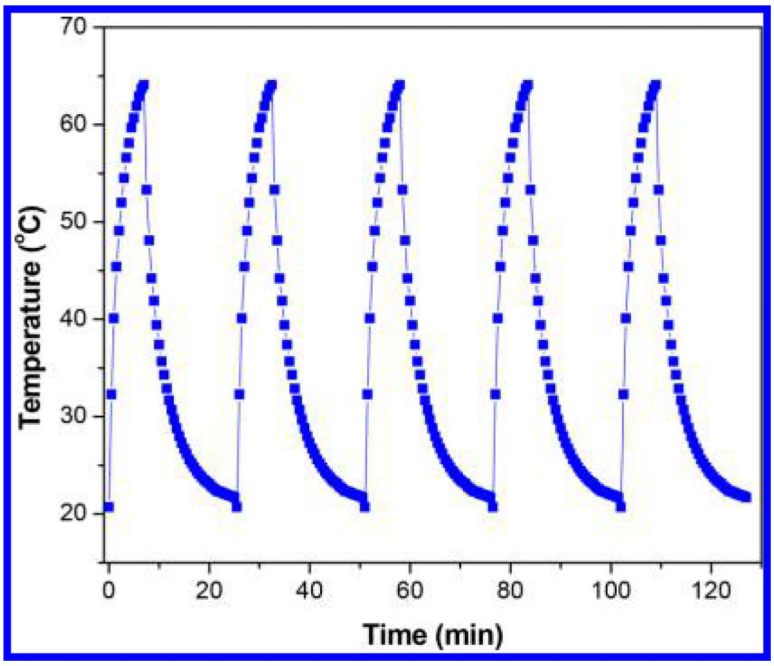

Figure 8.

Temperature variation measured for the aqueous dispersion of the CNTs-PAMAM/G4-CdS (1 mg/mL) for five cycles under illumination by a 980 nm laser.

Table 1.

Temperature of Samples Measured during Photothermal Effect

sample	concentration of aqueous dispersion (mg/mL)	initial temperature before irradiation with 980 nm laser (°C)	final temperature after irradiation with 980 nm laser for 7 min (°C)	ΔT ($T_{final} - T_{initial}$) (°C)
water		20.8	28.9	8.1
CNTs	1.00	20.5	50.0	29.5
CNTs-PAMAM/G1	1.00	20.5	53.4	32.9
CNTs-PAMAM/G2	1.00	20.4	55.2	34.8
CNTs-PAMAM/G3	1.00	20.2	58.4	38.2
CNTs-PAMAM/G4	1.00	20.3	62.1	41.8
CNTs-PAMAM/G4-CdS	1.00	20.7	64.1	43.4
CNTs-PAMAM/G4-CdS	0.50	20.5	62.5	42.0

Table 2.

Properties Used in Calculation of Photothermal Conversion Efficiency

sample	T_{max} (°C)	T_{surr} (°C)	$T_{max} - T_{surr}$ (°C)	A_{980}	η (%)
CNTs-PAMAM/G4	62.1	20.3	41.8	1.021	23
CNTs-PAMAM/G4-CdS	64.1	20.7	43.4	1.129	32